Journal of Science and Transport Technology
Journal homepage: https://jstt.vn/index.php/en

Evaluation of ABS braking performance for vehicles descending slopes under different road adhesion coefficients

Trung Kien Nguyen, Trong Hoan Nguyen*
Faculty of Automotive Engineering Technology, Dai Nam University

Article info
Type of article:
Original research paper

DOI:
https://doi.org/10.58845/jstt.utt.2026.en.6.5.180-196

***Corresponding author:**
Email address:
hoannt.cko@dainam.edu.vn

Received: 23/02/2026
Received in Revised Form: 18/05/2026
Accepted: 07/06/2026

Abstract: Braking safety on downhill roads with varying tire–road adhesion is a critical concern in vehicle dynamics. This paper evaluates the effectiveness of the Anti-lock Braking System (ABS) during downhill braking through a combined simulation and experimental approach. A longitudinal vehicle dynamics model is developed, integrating a driver model, vehicle body dynamics, wheel dynamics, and an ABS model employing a Fuzzy Logic controller. Simulation results are compared with experimental braking data to validate the model, assess controller performance, and evaluate ABS behavior on an actual vehicle. The comparison shows that braking performance parameters follow similar variation trends in both simulation and experiment; however, the Fuzzy controller maintains the wheel slip ratio within its optimal range with noticeably higher stability in simulation than in experiment. Using the validated model, braking performance from an initial speed of 60 km/h is investigated across different road adhesion coefficients and slope angles. When the adhesion coefficient decreases from 0.8 to 0.3, braking distance increases by 354.07% at an 8° slope and 725.50% at a 12° slope. Under low-adhesion conditions (φ = 0.3), increasing the slope from 8° to 12° raises braking distance by 121.16%, whereas under high-adhesion conditions (φ = 0.8), the increase is only 16.03%. These findings highlight the necessity of simultaneously accounting for road grade and adhesion coefficient when assessing ABS braking performance on downhill roads.

Keywords: anti-lock braking system (ABS), longitudinal dynamics, Fuzzy logic controller, tire–road adhesion coefficient, braking on sloped road.

1. Introduction

Braking safety is a fundamental requirement in vehicle design and operation, especially under adverse road conditions such as low adhesion coefficients or sloped surfaces. To evaluate braking performance, the principal criteria are commonly selected in accordance with FMVSS 135 standards, including braking distance, mean fully developed deceleration, stability, and controllability during braking [1]. The Anti-lock Braking System (ABS) was developed to maintain wheel slip within its optimal range, thereby improving braking efficiency and ensuring vehicle motion stability. Studies in vehicle dynamics have identified the nonlinear relationship between wheel slip ratio and longitudinal tire force within the tire–road contact patch, which constitutes a decisive factor governing braking characteristics and overall braking effectiveness of the vehicle [2-5].

On this basis, numerous studies have focused on developing braking dynamics models and proposing various ABS control strategies to

improve braking performance and stability. Conventional control methods such as PID and LQR have been widely applied due to their simple structure and ease of implementation; however, their control effectiveness often degrades significantly when road adhesion conditions vary substantially or when the system exhibits strong nonlinear characteristics [6,7]. To overcome these limitations, more advanced control approaches have been proposed, including sliding mode control, adaptive control, Model Predictive Control (MPC), and neural network–based methods. These approaches demonstrate the capability to enhance the accuracy and robustness of the ABS under complex operating conditions; nevertheless, they typically require precise mathematical models and high computational cost, creating challenges for implementation in real-time onboard control systems [8-11].

In this context, many studies have adopted Fuzzy and Neuro controllers due to their strong capability in handling nonlinearities, adapting to variations in adhesion conditions, and operating without requiring an exact mathematical model. Numerous investigations have demonstrated that applying Fuzzy control to the ABS can improve braking effectiveness and maintain wheel slip close to its optimal value under different road surface conditions [12-15]. However, in most of these works, the optimal slip value is commonly predefined or selected empirically, and the studies are mainly conducted under level road conditions, without fully considering the influence of road slope on braking characteristics and controller performance.

In addition to research focusing on standalone ABS control, several studies have expanded the scope by integrating ABS with other vehicle systems such as semi-active suspension systems, drivetrains, or steering systems to enhance overall vehicle stability during braking [16-19]. Furthermore, investigations on coordinating ABS with regenerative braking in electric and hybrid vehicles have attracted considerable attention in recent years, primarily aiming to improve energy recovery efficiency while ensuring braking safety [20-24]. Nevertheless, these studies largely concentrate on the individual effects of road adhesion coefficient or brake force distribution strategy, whereas the combined influence of adhesion coefficient and road slope on braking performance has not yet been quantitatively clarified.

Road slope alters the distribution of normal reaction forces and longitudinal forces acting on the wheels, thereby reducing braking effectiveness compared with the level road case [5]. However, simultaneously incorporating both road grade and surface adhesion conditions into braking dynamics models and ABS control algorithms remains limited. Moreover, many current studies mainly remain at the simulation level, whereas comparison and validation with actual braking experimental data have not been adequately addressed [25]. Therefore, developing a braking dynamics model that simultaneously considers the effects of road slope and adhesion coefficient, and is experimentally validated, is necessary to accurately evaluate the performance and reliability of the ABS under real operating conditions [26].

In this context, this paper proposes an approach combining simulation and experimentation to systematically investigate the longitudinal vehicle dynamics during downhill braking. A comprehensive braking dynamics model is developed, including a vehicle body dynamics model, a wheel dynamics model, and a braking system model, in which the braking system integrates a Fuzzy controller to regulate braking torque according to wheel slip. Unlike many previous studies, the optimal slip value is not predefined but is directly determined from hard braking experimental results on dry asphalt pavement, and subsequently employed as an input parameter for the control algorithm. Based on the developed model, the study quantitatively

examines the combined influence of road adhesion coefficient and slope angle on braking characteristics through simulation scenarios under various operating conditions. Furthermore, through direct comparison between simulation results and experimental data, the stability and effectiveness of the Fuzzy controller under downhill braking conditions are evaluated, thereby providing a quantitative foundation for analysis and design of ABS in a practical operating environment.

2. Theoretical background

During vehicle braking on a sloped road, the force diagram acting on the vehicle is illustrated in Fig. 1.

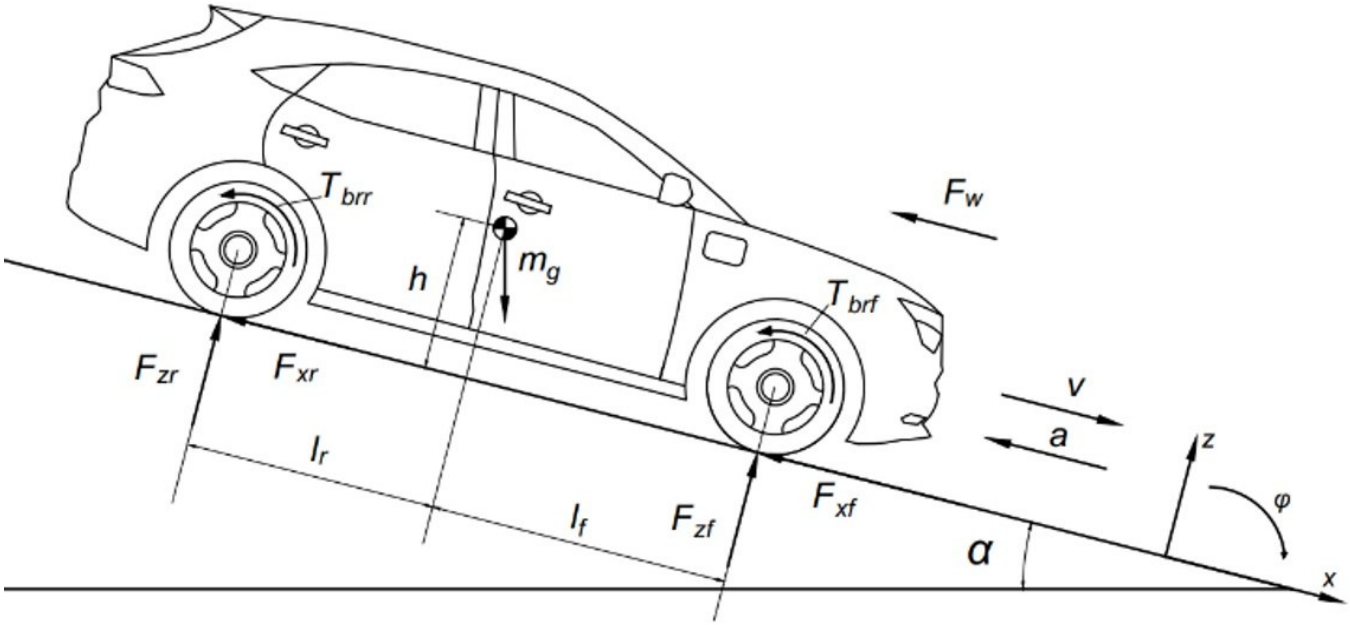


Fig. 1. Force diagram of a vehicle during braking on a sloped road

At that time, the longitudinal dynamic equation of the vehicle is expressed as follows [5]:

$$(m+m_e)\dot{v}=-(F_{xf}+F_{xr})-F_w+m.g.\sin\alpha \quad (1)$$

where: m – gross vehicle mass; m_e – equivalent mass accounting for rotating components (m_e = 0.05 m); u – vehicle velocity; F_{xf} , F_{xr} – longitudinal forces at the front and rear wheels, respectively; F_w - aerodynamic drag force.

The aerodynamic drag force acting on the vehicle during motion is calculated according to the following equation [5]:

$$F_W=\frac{1}{2}\rho C_W A v^2 \quad (2)$$

where: A - frontal area; ρ - air density (kg/m^3); C_w - aerodynamic drag coefficient.

During vehicle braking, under the action of inertial force, the vehicle weight is redistributed between the axles. Accordingly, the normal reaction forces acting on the front and rear axles are respectively expressed as follows:

$$F_{zf}=\frac{m.g.\cos(\alpha)}{(l_f+l_r)}.[l_r+h_w.\left(\tan(\alpha)-\frac{\dot{v}}{g}.\frac{1}{\cos(\alpha)}\right)] \quad (3)$$

$$F_{zr}=\frac{m.g.\cos(\alpha)}{(l_f+l_r)}.[l_f-h_w.\left(\tan(\alpha)-\frac{\dot{v}}{g}.\frac{1}{\cos(\alpha)}\right)] \quad (4)$$

Fig. 2 illustrates the force diagram acting on the wheel during braking [5]:

The rotational equation of motion of the wheel is expressed as follows:

$$J_w . \dot{\omega}=(F_x+F_f).r-T_{br} \quad (5)$$

where: T_{br} - braking torque at the wheel, J_w - moment of inertia of the wheel, F_f - rolling resistance force at the wheel, r - effective rolling radius of the wheel (m), ω – wheel angular velocity.

The rolling resistance force at each wheel is expressed as follows:

$$F_f= F_z . f \quad (6)$$

where: f – rolling resistance coefficient

The tire slip ratio during braking is defined as follows [10, 14]:

$$s=\left(\frac{\omega.r}{v}-1\right) \quad (-1<s<0) \tag{7}$$

Under each vehicle operating condition, the slip ratios of the front and rear wheels influence the traction coefficient. This coefficient is interpolated from experimental results [20] obtained on dry asphalt pavement, and the relationship between slip ratio and traction coefficient is illustrated in Fig. 3.

Accordingly, the longitudinal force at each wheel is calculated according to the following equation [20]:

$$F_x=F_z.\mu_s \tag{8}$$

where: μ_s – traction coefficient in Fig. 3.

3. Simulation Model and Experimental

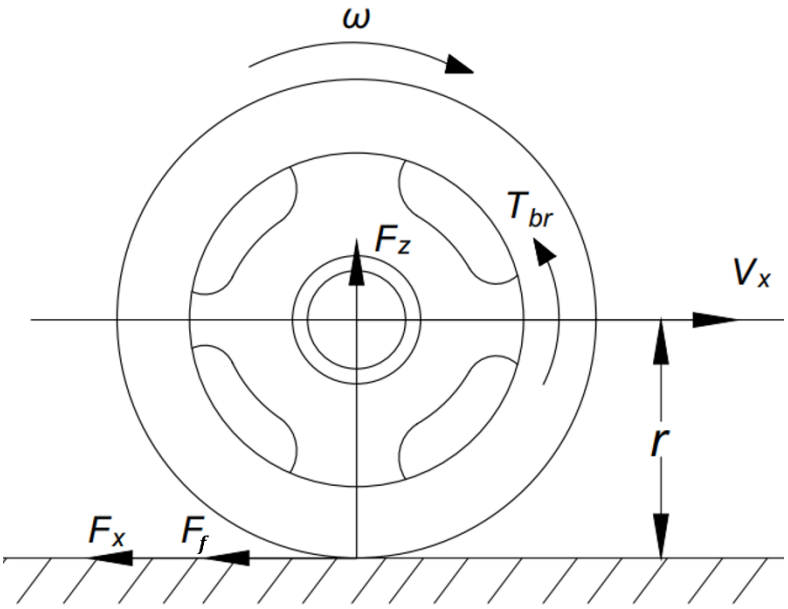


Fig. 2. Force diagram acting on the wheel

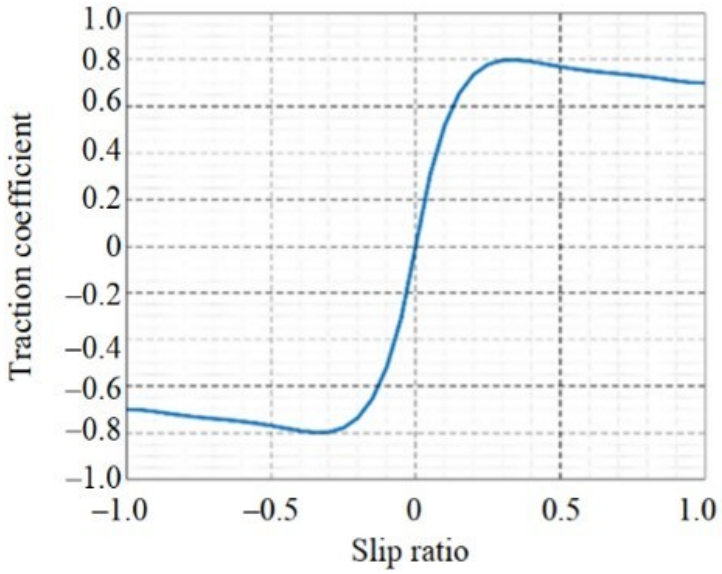


Fig. 3. Relationship between the traction coefficient and wheel slip ratio

3.1. Simulation Model and Simulation Scenarios

3.1.1. Simulation model

The simulation model of the vehicle braking process from an initial velocity v_0 on a road surface with slope angle α and adhesion coefficient φ was developed using specialized software, as shown in Fig. 4. The model comprises the main functional blocks, including the braking system model integrated with a Fuzzy controller, the front and

rear wheel dynamic models, and the vehicle body dynamic model.

The brake pedal input signal p_{br} from the driver model is transmitted to the brake torque distribution block, where the maximum braking torques at the front and rear axles, $T_{br_F_max}$ and $T_{br_R_max}$, are determined. These values, together with the wheel slip ratios s_F and s_R, are used as inputs to the Fuzzy brake torque controller. The controller output is the braking torque applied to each wheel. On that basis, the wheel model calculates dynamic quantities, where the slip *s* is fed back to the Fuzzy controller, whereas the longitudinal force F_x is input into the vehicle body dynamics model to determine the braking distance S, velocity v_x, and braking acceleration a. The input parameters of the model are referenced from the VF8 electric vehicle model and are listed in Table 1 [27].

a. Braking system model with the Fuzzy controller

The maximum braking torque values at the front and rear axles, as well as the brake pedal input level, are determined according to the brake pedal position p_{br}:

$$T_{br_FL_max}=T_{br_FR_max}=\frac{1}{2}.p_{br}.m\ .g\ .\ a.r \quad (9)$$

$$T_{br_RL_max}=T_{br_RR_max}=\frac{1}{2}.p_{br}.m\ .g\ .\ b.r \quad (10)$$

where: a,b: brake torque distribution coefficients for the front and rear axles, respectively.

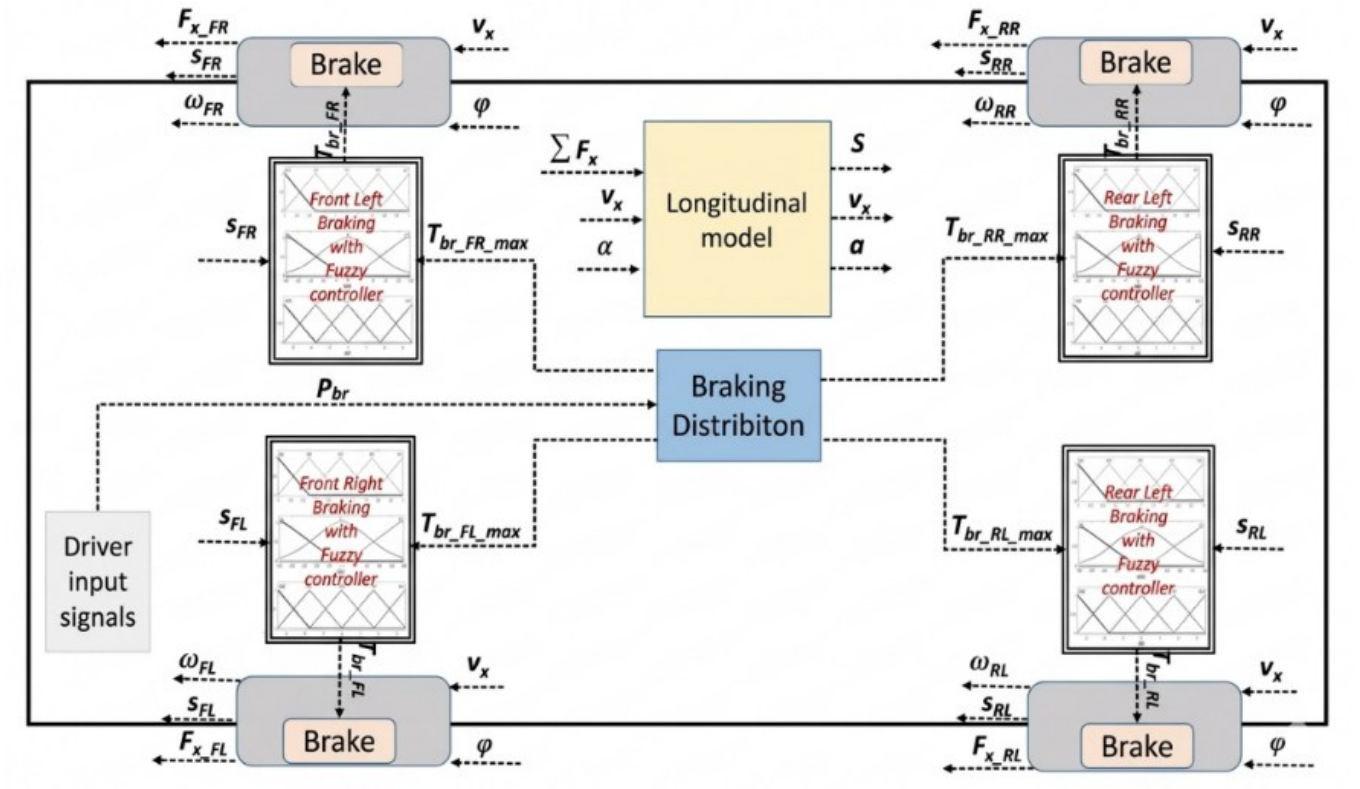


Fig. 4. Block diagram of the braking system model with the Fuzzy controller

Table 1. Basic parameters of the reference vehicle

Parameter	Symbol	Value	Unit
Vehicle weight	G	29400	N
Distance from the front axle to the vehicle center of gravity	l_f	1504.5	mm
Distance from rear axle to vehicle center of gravity	l_r	1445.5	mm
Wheelbase	L	2950	mm
Height of the vehicle center of gravity	h_w	650	mm
Dynamic rolling radius of the wheel	r	360.5	mm

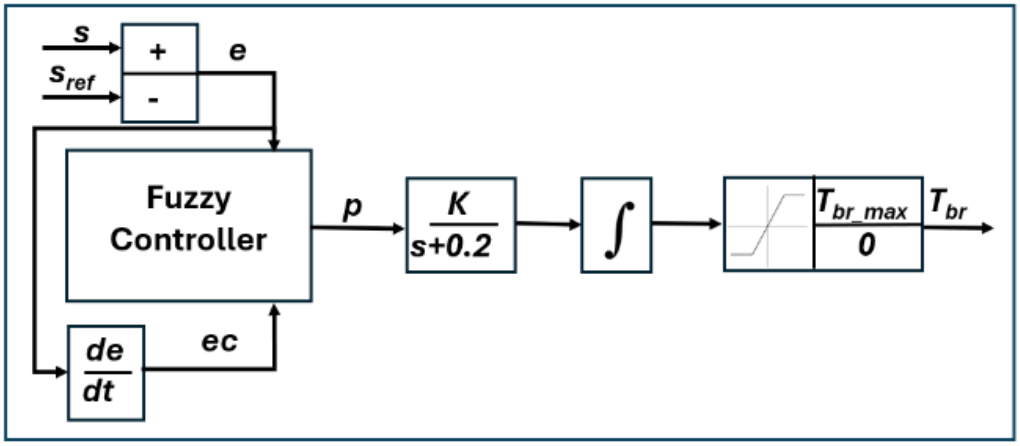


Fig. 5. Block diagram of the brake torque control model based on slip ratio

During vehicle braking, in order to prevent wheel lock-up, the Fuzzy controller calculates the optimal braking torque at each wheel, T_{br}. The inputs of this controller are the error e and the derivative of the error e_c, where e represents the deviation between the desired slip ratio s_{opt} and the actual slip ratio s, as illustrated in Fig. 5. Block diagram of the brake torque control model based on slip ratio.

The input and output signal regions of the Fuzzy controller are illustrated in Fig. 6. The two input variables, namely the slip error e and the derivative of the error e_c, are fuzzified into linguistic sets and interconnected through Fuzzy control rules. The control signal p varies according to the corresponding inference rules to adaptively adjust the braking torque, thereby maintaining the slip ratio close to its optimal value and ensuring braking effectiveness as well as stability [18].

where: NL – Negative Large; NS - Negative Small; ZE - Zero; PS - Positive Small; PL - Positive Large; DPL - Decrease Pressure Large; DPS - Decrease Pressure Small; HOLD - Hold Pressure; IPS - Increase Pressure Small; IPL - Increase Pressure Large.

The control rules of the Fuzzy controller follow the rule base defined below [14]:

1. If (e is NL) and (ec is NL), then (p is DPL)
2. If (e is NL) and (ec is NS), then (p is DPS)
3. If (e is NL) and (ec is ZE), then (p is HOLD)
4. If (e is NS) and (ec is NL), then (p is DPL)
5. If (e is NS) and (ec is ZE), then (p is DPS)
6. If (e is NS) and (ec is PL), then (p is HOLD)
7. If (e is ZE) and (ec is NS), then (p is DPS)
8. If (e is ZE) and (ec is ZE), then (p is HOLD)
9. If (e is ZE) and (ec is PS), then (p is IPS)
10. If (e is PS) and (ec is NL), then (p is HOLD)
11. If (e is PS) and (ec is NS), then (p is IPS)
12. If (e is PS) and (ec is ZE), then (p is IPL)
13. If (e is PL) and (ec is NS), then (p is HOLD)
14. If (e is PL) and (ec is ZE), then (p is IPS)
15. If (e is PL) and (ec is PL), then (p is IPL)

The above control rules are established to describe the operation of the Fuzzy controller in response to variations of the slip error e and the error derivative e_c. When both e and e_c take negative values (NL, NS), meaning that the slip magnitude exceeds the allowable level and tends to increase, the controller prioritizes the DPL and DPS rules to significantly reduce the braking torque, thereby bringing the slip ratio back to the safe region. Conversely, when e and e_c take positive values (PS, PL), indicating that the slip ratio is lower than the optimal value and tends to decrease, the system applies the IPS or IPL rules to increase the braking torque in order to raise the slip ratio toward the target value. For equilibrium or transitional cases (ZE), the controller applies the

HOLD rule or slight adjustment levels (DPS, IPS) to maintain braking torque stability when the slip ratio remains within the optimal region. The calculated braking torque must lie within the limit range [0, T_{br_max}] to comply with the braking system design specifications.

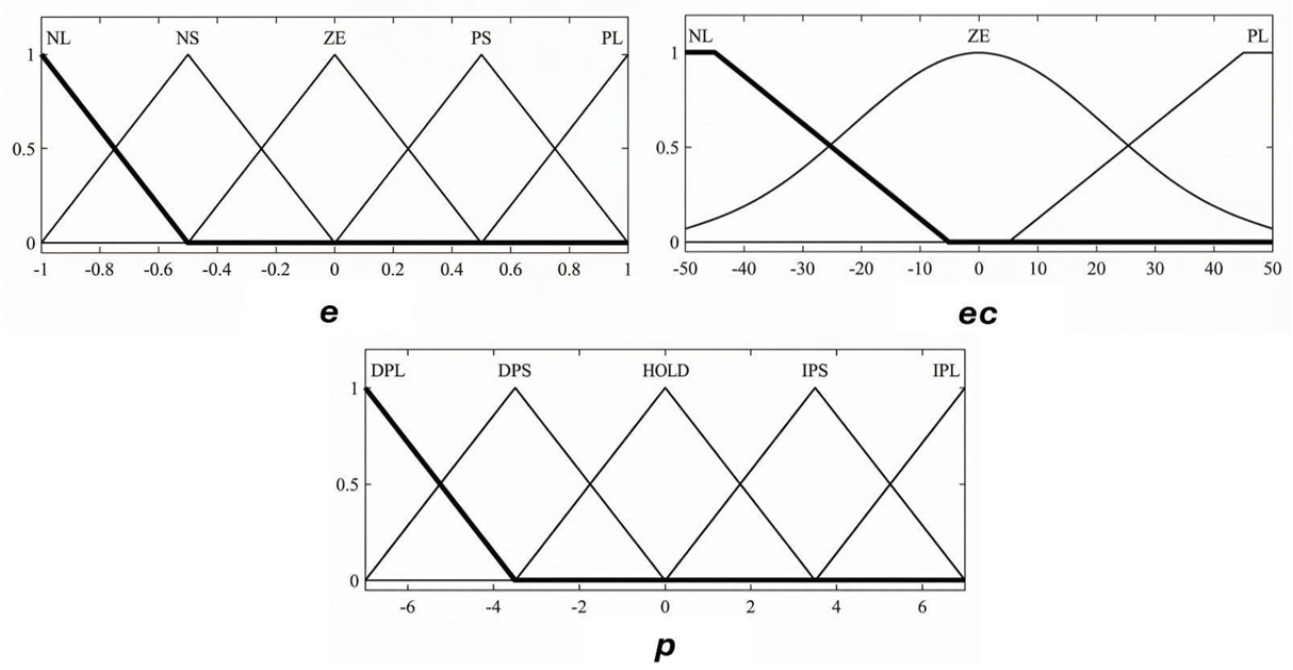


Fig. 6. Input and output signal regions of the Fuzzy controller

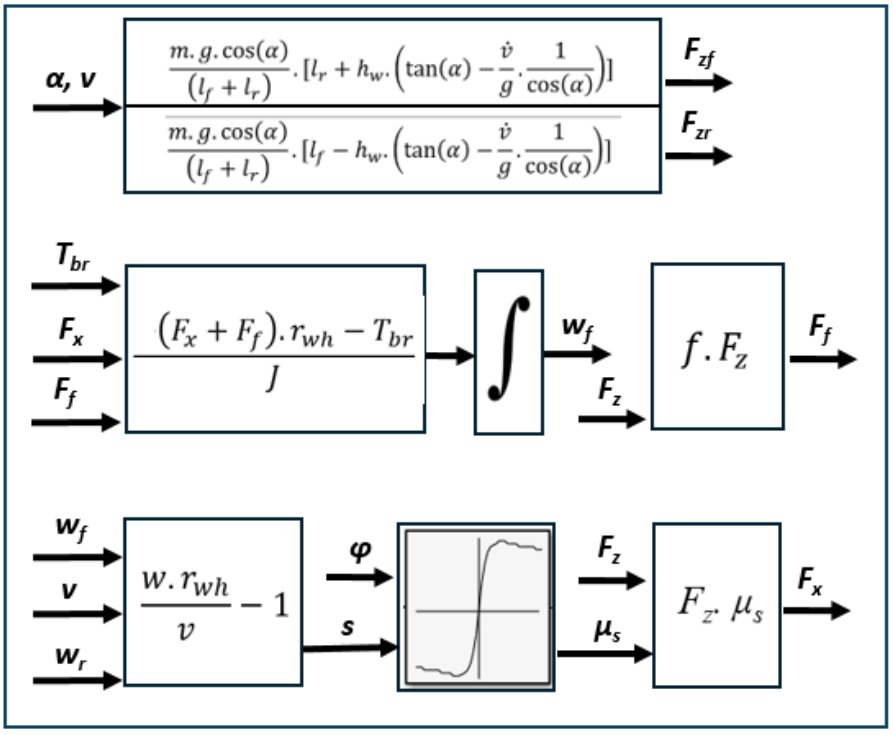


Fig. 7. Schematic diagram of the wheel dynamic model during braking

b. Wheel dynamic model

The wheel dynamic model takes as inputs the slip ratio, the braking torque at each wheel T_{br}, and the tire–road adhesion coefficient φ.

Based on the tire model identified from experimental results shown in Fig. 3 and the wheel dynamic equation (5), the longitudinal force at each wheel is determined and transmitted to the vehicle body dynamic model. The schematic diagram of the wheel dynamic model is illustrated in Fig. 7.

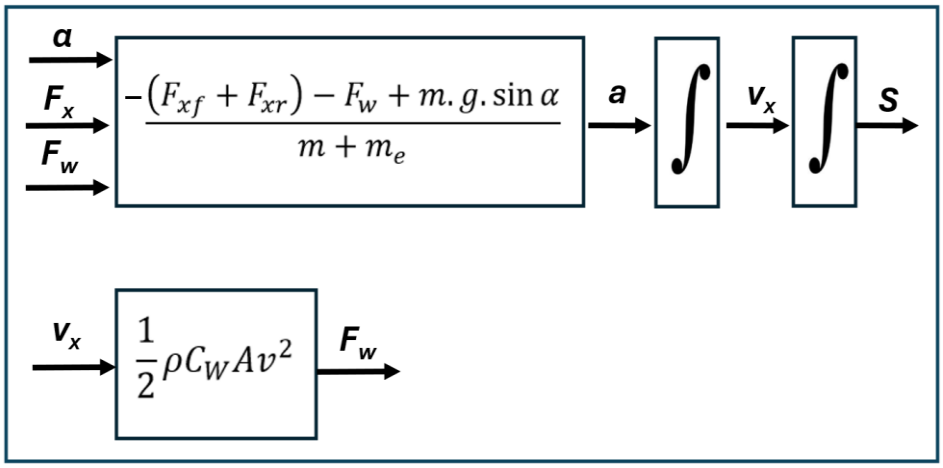


Fig. 8. Schematic diagram of the vehicle body dynamic model

c. Longitudinal vehicle body dynamic model

The longitudinal forces F_x at each wheel, determined from the wheel model, are transmitted to the vehicle body dynamic model to calculate the braking performance indicators during braking, namely the braking deceleration a and the braking distance S. The schematic diagram of the vehicle body dynamic simulation model is illustrated in Fig. 8.

3.1.2. Simulation scenarios

Table 2. Simulation Scenarios

Initial velocity v_o (km/h)	Slope angle α (°)	Brake pedal level p_{br}	Adhesion coefficient φ		
			0.3	0.5	0.8
50.40	6.8	- 0.32	-	-	x
64.26	6.8	-1	-	-	x
60	8	-1	x	x	x
	10	-1	x	x	x
	12	-1	x	x	x

- = Unsimulated

x = Simulated

To investigate the longitudinal dynamics of the vehicle during braking, the primary parameters considered include braking time t, braking distance S, braking deceleration a, and the slip ratios of the front and rear wheels s_F and s_R. Based on the developed model, the braking process is simulated from an initial speed of 60 km/h until the vehicle comes to a complete stop with a brake pedal input level of p_{br}=-1, corresponding to hard braking, under road surface conditions with different adhesion coefficients (0.3, 0.5, and 0.8) and varying slope angles (8°, 10°, and 12°). In addition, the simulation scenarios are also configured for two braking modes: mild braking at a speed of 50.4 km/h and hard braking at a speed of 64.26 km/h on a high-adhesion road surface with an adhesion coefficient of 0.8 and a slope angle determined from experimental results of 6.8°. The simulation results of these two cases are compared with experimental data to validate the accuracy of the developed simulation model and the optimal slip value s_{opt}. The simulation scenarios are presented in Table 2.

3.2. Experimental Investigation

The experimental scenario was established under two braking conditions, namely light braking and emergency braking, conducted on dry asphalt pavement with a road slope of α = 6.8°, in order to evaluate the reliability of the simulation model, determine the optimal slip ratio s_{opt} of the wheel

during emergency braking to serve as an input for the Fuzzy controller, and assess the performance of the proposed Fuzzy control algorithm. The experimental procedure is illustrated in Fig. 9. At point A, the vehicle initiates the braking process with an initial longitudinal velocity v_0 and longitudinal acceleration a=0(m/s²). The driver applies the brake pedal with a braking input of p_{br}=-1 for emergency braking and p_{br}=-0.32 for light braking. At the moment the driver depresses the brake pedal, the brake switch sensor generates a signal confirming the brake pedal actuation and transmits it to the central data acquisition and processing unit (Dewe), thereby triggering the data recording process. Throughout the braking event, the measured signals include braking distance S (m), braking deceleration a(m/s²), and vehicle longitudinal velocity v (m/s), which are obtained via the S-motion sensor. Meanwhile, the angular velocities of the wheels ω(rad/s) are measured over time using WPT sensors. The braking process concludes at point B, when the vehicle longitudinal velocity reaches v=0(km/h), at which point data acquisition and storage of the experimental results are completed [28].

The specifications of the experimental measurement equipment are summarized in Table 3 [28]:

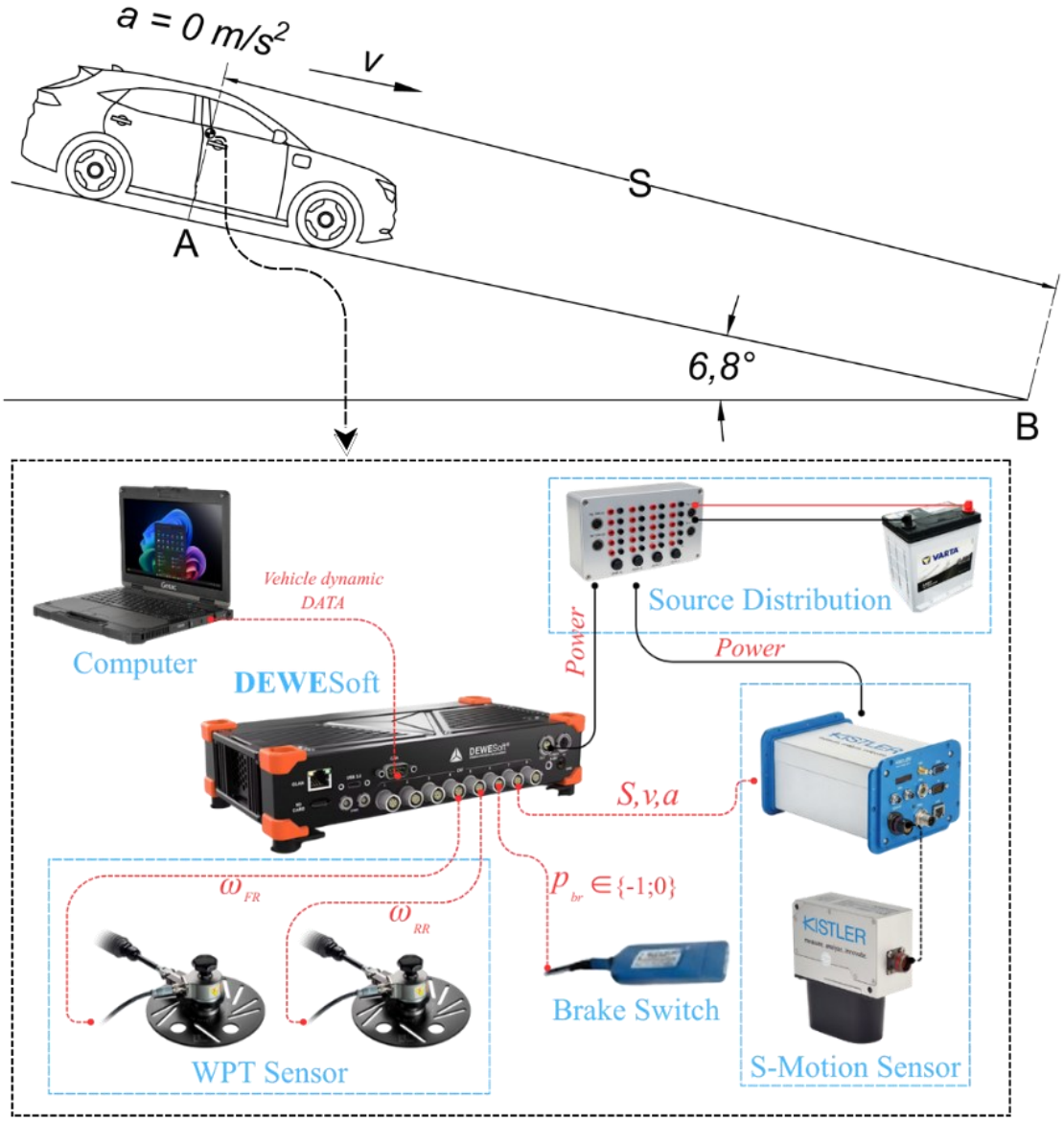


Fig. 9. Diagram of the Experimental Procedure

Table 3. Parameters of experimental equipment.

Sensor	Measured Parameter	Measurement Range	Resolution
WPT	n	±6000 (rpm)	10 … 5000 (pulses/rev)
S-Motion	S	-	≤1 mm
	v	±0.1…250(km/h)	<±0.2%FSO
	a	±18g	±0.15%FSO
SW-50G	α	±90°	±0.1°

n = number of wheel revolutions
FSO = Full Scale Output
g = gravitational acceleration



Fig. 10. Inclination Angle of the Experimental Road.



Fig. 11. Experimental Equipment Installed on the Tested Vehicle

Images illustrating the method used to determine the road slope angle, as well as the experimental equipment installed on the actual test vehicle, are presented in Fig. 10 and Fig. 11, respectively.

4. Results and Discussion

4.1. Simulation Model Validation

The braking torque values at the front and rear axles are determined as T_{br_F}= 1800 Nm and T_{br_R}= 1000 Nm, respectively. These values were

obtained through calculation and experimental measurement under the light braking condition with an initial braking speed of v_0= 50.40 km/h on dry asphalt at a road slope angle of 6.8°, corresponding to a brake pedal input of p_{br}= -0.32. The brake pedal input p_{br}= -0.32 is applied to the simulation model together with the identified vehicle parameters to reproduce the light braking process on the inclined road. The simulated braking torque values at the front and rear wheels closely follow the experimentally measured torque values, as illustrated in Fig. 12 (a) and Fig. 12 (b). Based on this, the comparison results of braking distance S(m) and vehicle longitudinal velocity v(m/s) between simulation and experimental data are presented in Fig. 12(c) and Fig. 12(d).

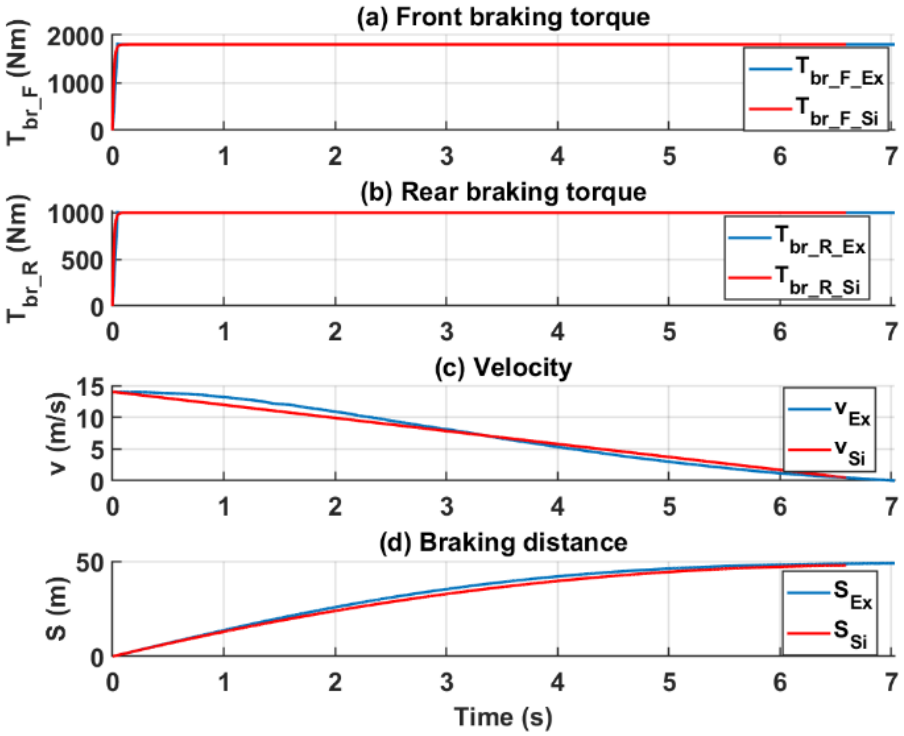


Fig. 12. Dynamic Parameters during Mild Braking at an Initial Speed of 50.40 km/h, Adhesion Coefficient 0.8, and Road Slope Angle 6.8°

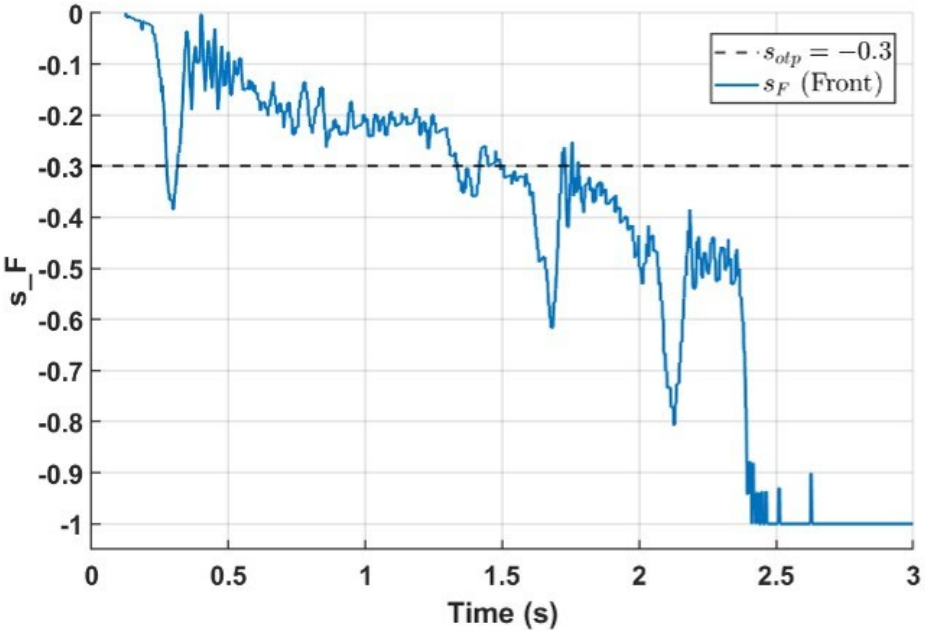


Fig. 13. Optimal Wheel Slip Ratio Determined from Experimental Results

The braking time determined from the experiment and simulation is t_{Ex} = 7.035 s and t_{Si} = 6.595 s, respectively, corresponding to a deviation of 7%, while the braking distance is S_{Si} = 47.74 m and S_{Ex} = 48.84 m, with a discrepancy of 2.3%. These results indicate that the simulation model exhibits a high level of agreement with the operating characteristics of the braking system on the reference vehicle under the investigated conditions.

4.2. Investigation of ABS Braking Performance under Different Road Surface Conditions

Fig. 13 presents the slip ratio of the front wheel obtained from the experimental test under hard braking conditions. The optimal slip value s_{opt}= -0.306 is determined through time-domain analysis [29] within the interval in which the ABS operates stably (0.5 – 2.5 s), and this value is subsequently used as an input parameter for the Fuzzy controller.

The graphs in Fig. 14 illustrate the dynamic braking characteristics of the vehicle obtained from both experimental tests and simulation at an initial braking speed of v_0=64.26 km/h, on a road with a slope angle of 6.8° and an adhesion coefficient of 0.8. The two principal indicators used to evaluate braking performance are braking time t(s) and braking distance S(m). The comparison results between experiment and simulation show strong agreement, as presented in Fig. 14. The braking time determined experimentally is t_{Ex}=3.032s, while the simulated value is t_{Si}=2.93s, corresponding to a deviation of approximately 3.36%. The experimental braking distance reaches S_{Ex}=25.191m, compared to the simulated distance S_{Si}=27.285m, resulting in a deviation of approximately 8.31%. The relatively small discrepancies in both braking distance and braking time between simulation and experimental results confirm the applicability of the developed simulation model for evaluating and predicting vehicle braking performance on downhill roads.

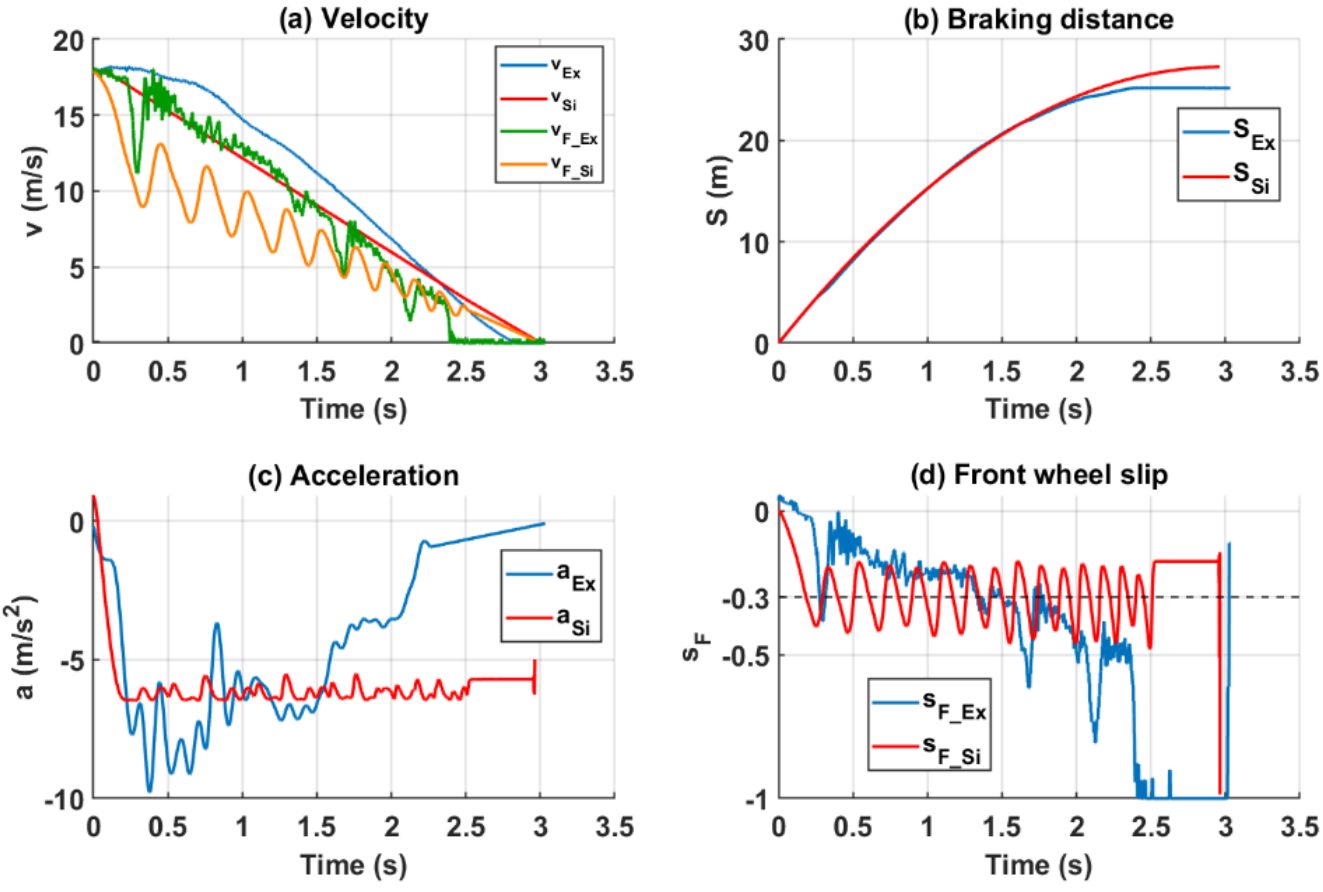


Fig. 14. Vehicle Dynamic Parameters during Emergency Braking

Table 4. Simulation Results

φ	α (°)	t (s)	S (m)	a_{max} (m/s^2)	a_{ave} (m/s^2)	s_F	s_R
0.3	8	13.125	110.113	-1.649	-1.265	-0.430	-0.277
	10	17.821	149.560	-1.313	-0.931	-0.436	-0.276
	12	27.896	233.618	-0.976	-0.596	-0.442	-0.276
0.5	8	5.387	45.639	-3.494	-3.085	-0.300	-0.276
	10	6.074	51.310	-3.144	-2.746	-0.303	-0.279
	12	6.903	58.674	-2.792	-2.407	-0.302	-0.278
0.8	8	2.826	24.250	-6.477	-5.923	-0.282	-0.280
	10	3.064	26.402	-5.899	-5.344	-0.277	-0.393
	12	3.337	28.300	-5.528	-4.979	-0.288	-0.404

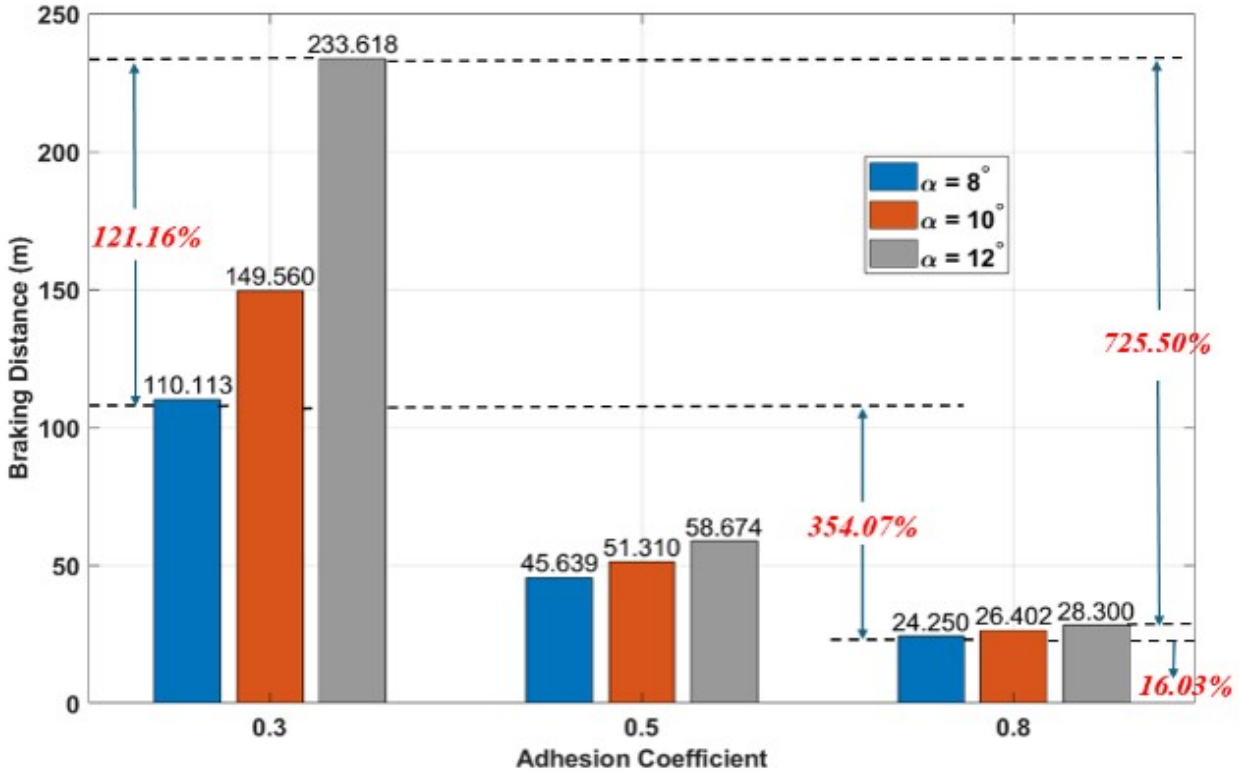


Fig. 15. Influence of Road Adhesion Coefficient and Road Slope Angle on Braking Distance

In the experimental case, the slip ratio was maintained stably around the mean value $\bar{s}_{Ex}$ = -0.3055, which is highly consistent with the average slip obtained from the simulation, $\bar{s}_{Si}$ = -0.3060. However, the slip ratio in the simulation, s_{Si}, exhibited a relatively small oscillation amplitude, with Δs_{Si} =0.289, corresponding to only about 30.8% of the experimental amplitude Δs_{Ex} = 0.940. In addition, the variance of the slip ratio in the simulation was approximately 27.5% of that observed in the experiment. These results indicate that the magnitude of oscillation and temporal variation of the slip ratio s in the simulation are significantly lower than those measured experimentally, reflecting the capability of the Fuzzy controller to maintain the slip ratio around the optimal operating value s_{opt} = -0.3 (Fig. 14(d)). When the slip ratio is maintained stably around the optimal value, the longitudinal force at each wheel also varies less over time, resulting in a more stable deceleration response. This trend is clearly illustrated in the deceleration plot. The analysis results show that, in the simulation, the deceleration oscillates around the mean value $\bar{a}_{Si}$

= -6.208 m/s^2 with a relatively small amplitude Δa_{Si} = 0.964. In contrast, in the experimental case, the deceleration fluctuates around the mean value $\bar{a}_{Ex}$ = -5.399 m/s^2 with a significantly larger amplitude Δa_{Ex} =9.063. The comparison indicates that the deceleration oscillation amplitude in the simulation is only about 10.64% of that observed in the experiment, reflecting better control of temporal acceleration variation in the simulation. In addition, the acceleration variance in the simulation reaches $\sigma^2_{a,Si}$ = 0.051, corresponding to only about 0.95% of the experimental acceleration variance $\sigma^2_{a,Ex}$ = 5.362. These results demonstrate that the deceleration in the simulation is considerably more stable than in the experiment, consistent with the stable behavior of the slip ratio shown in Fig. 14(d). This confirms the effectiveness of the developed Fuzzy controller; moreover, the stability of the deceleration a(m/s²) strongly depends on the slip ratio s.

Table 4 presents the simulation results of the braking process corresponding to the developed scenarios, in which the parameters used to evaluate braking performance include braking distance S, braking time t, maximum deceleration a_{max}, average deceleration a_{ave}, and the average slip ratios of the front and rear wheels s_F, s_R. The results indicate that the dynamic parameters vary consistently with changes in the road adhesion coefficient and road slope angle. As the adhesion coefficient increases, both braking time and braking distance tend to decrease, while the magnitudes of maximum and average deceleration increase. Under conditions of low adhesion or large slope angles, although the capability to control brake torque according to the optimal slip ratio is maintained, braking performance is limited by the available tire–road adhesion and the gravitational component along the longitudinal direction, resulting in prolonged braking time and increased braking distance. This demonstrates that the braking system employing the Fuzzy control algorithm maintains operation near the optimal tire adhesion region, ensuring stability and braking effectiveness under various road surface conditions.

Fig. 15 illustrates the dependence of braking performance, characterized by the braking distance S, on the road adhesion coefficient and the road slope angle. The simulation results indicate that as the road adhesion coefficient decreases, the braking distance increases significantly under all considered slope conditions. At a slope angle of 8°, when the adhesion coefficient decreases from 0.8 to 0.3, the braking distance increases from 24.250 m to 110.113 m, corresponding to an increase of 354.07%. Similarly, at a slope angle of 12°, the braking distance increases from 28.300 m to 233.618 m, corresponding to an increase of 725.50%. These results demonstrate that road adhesion conditions have a substantial influence on braking performance, particularly in the case of steep downhill roads. When examining the influence of road slope under the same adhesion condition, the impact of slope angle on braking performance exhibits a clear variation across different adhesion levels. On a low-adhesion surface with a coefficient of 0.3, when the slope angle increases from 8° to 12°, the braking distance rises from 110.113 m to 233.618 m, corresponding to an increase of 121.16%. In contrast, on a high-adhesion surface with a coefficient of 0.8, when the slope angle increases from 8° to 12°, the braking distance increases only from 24.250 m to 28.300 m, corresponding to a 16.03% increase. This indicates that the influence of road gradient is significantly attenuated under good tire–road adhesion conditions.

5. Conclusions

The study provides quantitative results highlighting the critical importance of simultaneously considering road slope and surface adhesion coefficient when evaluating ABS braking performance. The model was validated through

direct comparison with actual braking experimental data under corresponding operating conditions. The comparison results indicate that the deviation between braking performance indices obtained from simulation and experiment is less than 10%, thereby confirming the accuracy and reliability of the proposed dynamic model and control algorithm. In addition, the Fuzzy controller demonstrates the capability to maintain wheel slip fluctuating around the optimal value s_{opt} = -0.3, with higher stability than that observed in experimental results. Based on the developed model, a total of eleven braking simulation cases were conducted under different adhesion coefficients and slope angles, combined with two experimental cases for validation. The investigation results show that when the adhesion coefficient decreases from 0.8 to 0.3, the braking distance increases significantly, reaching 354.07% at an 8° slope and 725.50% at a 12° slope. Furthermore, under low adhesion conditions of 0.3, when the slope angle increases from 8° to 12°, the braking distance increases by 121.16%, whereas under good adhesion conditions of 0.8, the increase is only approximately 16.03%. These findings can serve as a reference basis for the development, calibration, and evaluation of ABS control strategies under more complex operating conditions in future studies, particularly for downhill braking scenarios with varying adhesion conditions.

Declaration of Generative AI

During the preparation of this work, the authors used ChatGPT in order to improve the readability and English grammar of the manuscript. After using this tool, the authors reviewed and edited the content as needed and take full responsibility for the content of the published article.

References

[1] National Highway Traffic Safety Administration (NHTSA). (2005). Laboratory test procedure for FMVSS 135: Light vehicle brake systems. U.S.

[2] T.K. Bera, K. Bhattacharya, A.K. Samantaray. (2011). Evaluation of antilock braking system with an integrated model of full vehicle system dynamics. *Simulation Modelling Practice and Theory*, 19(10), 2131–2150. https://doi.org/10.1016/j.simpat.2011.07.002

[3] X. Zhang, Y. Xu, M. Pan, F. Ren. (2014). A vehicle ABS adaptive sliding-mode control algorithm based on the vehicle velocity estimation and tyre/road friction coefficient estimations. *Vehicle System Dynamics*, 52(4), 475–503. https://doi.org/10.1080/00423114.2013.864775

[4] M. Ulum, D.A. Patriawan, M. Nizar. (2022). Modeling and performance testing of anti-lock braking system (ABS) with variation of road friction coefficient to braking distance. *Rekayasa: Journal of Science and Technology*, 15(3), 340–345. https://doi.org/10.21107/rekayasa.v15i3.16561

[5] R.N. Jazar. (2017). Vehicle dynamics: Theory and application (2nd ed.). *Springer*.

[6] S.A. Abd El-Fatah, A.-N. Sharkawy, A.O. Moaaz, N.M. Ghazaly. (2021). A comparative study of different control methods for anti-lock braking system (ABS). *SVU-International Journal of Engineering Sciences and Applications*, 2(1), 27–34. https://doi.org/10.21608/svusrc.2021.65855.1007

[7] A.T. Nugraha, O.D. Pratiwi, R.F. As'ad, V.A. Athavale. (2022). Brake current control system modeling using linear quadratic regulator (LQR) and proportional integral derivative (PID). *Indonesian Journal of Electronics, Electromedical Engineering, and Medical Informatics*, 4(2), 85–93. https://doi.org/10.35882/ijeeemi.v4i2.141

[8] J.S. Esmaeili, A. Başçi, A. Farnam. (2023). Design and verification of offline robust model predictive controller for wheel slip control in ABS brakes. *Machines*, 11(8), 803. https://doi.org/10.3390/machines11080803

[9] M.F. Abdullah, G.A.A. Qasem, M. Farid, H.S. Lim, C.P. Lee, N. Alsakkaf. (2025). Adaptive control techniques for improving anti-lock braking system performance in diverse friction scenarios. *International Journal of Electrical and Computer Engineering*, 15(1), 260–279. https://doi.org/10.11591/ijece.v15i1.pp260-279

[10] Y. Li, H. Li. (2024). A study on the vehicle antilock system based on adaptive neural network sliding mode control. *Mathematical Problems in Engineering*, 2024, 3359266. https://doi.org/10.1155/2024/3359266

[11] M.F. Abdullah, G.A. Qasem, M. Farid. (2025). An enhanced ABS braking control system with autonomous vehicle stopping. *World Electric Vehicle Journal*, 16(7), 400. https://doi.org/10.3390/wevj16070400

[12] J. El-bakkouri, H. Ouadi, A. Saad. (2022). Adaptive neuro fuzzy inference system based controller for electric vehicle's hybrid ABS braking. *IFAC PapersOnLine*, 55(12), 371–376. https://doi.org/10.1016/j.ifacol.2022.07.340

[13] J. Pramudijanto, A. Ashfahani, R. Lukito. (2018). Designing neuro-fuzzy controller for electromagnetic anti-lock braking system (ABS) on electric vehicle. *Journal of Physics: Conference Series*, 974(1), 012055. https://doi.org/10.1088/1742-6596/974/1/012055

[14] G.A.A. Qasem, M.F. Abdullah, M. Farid, Y.A. Bakhuraisa. (2025). Enhancing anti-lock braking system performance using fuzzy logic control under variable friction conditions. *Symmetry*, 17, 1692. https://doi.org/10.3390/sym17101692

[15] G.A.A. Qasem, M.F. Abdullah. (2024). Anti-lock braking systems: A comparative study of control strategies and their impact on vehicle safety. *International Research Journal of Innovations in Engineering and Technology*, 8(9), 131–143. https://doi.org/10.47001/IRJIET/2024.809016

[16] H.A. Hamersma, P.S. Els. (2014). Improving the braking performance of a vehicle with ABS and a semi-active suspension system on a rough road. *Journal of Terramechanics*, 56, 91–101. https://doi.org/10.1016/j.jterra.2014.09.004

[17] Z. Zhao, L. Zhang, X. Ding, Z. Zhang, S. Li, L. Gu. (2024). Integrated active suspension and anti-lock braking control for four-wheel-independent-drive electric vehicles. *Chinese Journal of Mechanical Engineering*, 37, 20. https://doi.org/10.1186/s10033-024-00997-8

[18] K. Bayar. (2022). Active motor damping strategy for driveline vibrations of a hybrid electric vehicle during ABS operation. *Proceedings of the Institution of Mechanical Engineers, Part D: Journal of Automobile Engineering, pp. 1–12.* https://doi.org/10.1177/09544070221114678

[19] N. Zhang, J. Wang, Z. Li, S. Li, H. Ding. (2022). Multi-agent-based coordinated control of ABS and AFS for distributed drive electric vehicles. *Energies*, 15(5), 1919. https://doi.org/10.3390/en15051919

[20] L.V. Nghia, D.H. Phuc, N.T. Hoan, S.V. Kharitonchik, V.A. Kusyak. (2023). Research of regenerative braking strategy for electric vehicles. *Energetika*. *Proceedings of CIS Higher Education Institutions and Power Engineering Associations*, 66(2), 105–123. (in Russian). https://doi.org/10.21122/1029-7448-2023-66-2-105-123

[21] J. Yong, Y. Yi, Z. Zhang, N. Feng, W. Li. (2024). Integrated control of anti-lock and regenerative braking for in-wheel-motor-driven electric vehicles. *Complex Engineering Systems*, 4(1), 2. https://doi.org/10.20517/ces.2023.36

[22] T. Wu, F. Wang, P. Ye. (2023). Regenerative braking strategy of dual-motor EV considering energy recovery and brake stability. *World Electric Vehicle Journal*, 14(1), 19. https://doi.org/10.3390/wevj14010019

[23] Q. Xu, C. Zhou, H. Huang, X. Zhang. (2021). Research on the coordinated control of

regenerative braking system and ABS in hybrid electric vehicle based on composite structure motor. *Electronics*, 10(3), 223. https://doi.org/10.3390/electronics10030223

[24] C. Tu, L. Zhang. (2022). Research on kinetic energy recovery of energy vehicle ABS solenoid valve based on the ELM deep learning model. *Computational Intelligence and Neuroscience*, 2022, 6571085. https://doi.org/10.1155/2022/6571085

[25] A.F. Geleta, M. Gopal, M.T. Lemi. (2024). Vehicle anti-lock brake system—dynamic modeling and simulation based on MATLAB Simulink and CarSim. *Research on Engineering Structures and Materials*, 10(2), 495–511. https://doi.org/10.17515/resm2023.22me0601rs

[26] S. Sumardi, M. Harly, M. Marji. (2020). Braking and acceleration mapping control for autonomous overtaking to avoid fatality crash in undivided road. *Journal of Physics: Conference Series*, 1700(1), 012037. https://doi.org/10.1088/1742-6596/1700/1/012037

[27] Euro NCAP. (2023). VinFast VF8 – safety rating. https://www.euroncap.com/assessments/vinfast/vf8/1008/ (accessed 26 January 2026).

[28] Kistler Group. (2024). Vehicle testing solutions: Correvit S-Motion optical sensors, WPT wheel pulse transducers, and brake trigger switches for dynamic performance evaluation. Technical documentation, https://www.kistler.com (accessed 26 January 2026).

[29] N.Q. Trung, P.V. Hiep, N.V. Vinh, B.H. Hai, N. T.P. Hoa, B.T.K. Thoa. (2023). Signal processing and digital filtering, Vol. 1: Basic program (Book 1). Hanoi University of Science and Technology Publishing House. (in Vietnamese).